frontiers | Frontiers in Physics

TYPE Original Research
PUBLISHED 07 June 2023
DOI 10.3389/fphy.2023.1184103

OPEN ACCESS

EDITED BY
Alberto Martinez Torres,
University of São Paulo, Brazil

REVIEWED BY
Feng-Kun Guo,
Chinese Academy of Sciences (CAS), China
Alessandro Pilloni,
National Institute of Nuclear Physics of Rome, Italy

*CORRESPONDENCE
Hua-Xing Chen,
hxchen@seu.edu.cn
Er-Liang Cui,
erliang.cui@nwafu.edu.cn

RECEIVED 11 March 2023
ACCEPTED 22 May 2023
PUBLISHED 07 June 2023

CITATION
Dong R-R, Su N, Chen H-X and Cui E-L (2023), QCD sum rule study on the fully strange tetraquark states of $J^{PC} = 2^{++}$. *Front. Phys.* 11:1184103. doi: 10.3389/fphy.2023.1184103

QCD sum rule study on the fully strange tetraquark states of $J^{PC} = 2^{++}$

Rui-Rui Dong[1], Niu Su[1], Hua-Xing Chen[1]* and Er-Liang Cui[2]*

[1]School of Physics, Southeast University, Nanjing, China, [2]College of Science, Northwest A&F University, Yangling, China

We apply the QCD sum rule method to systematically study the fully strange tetraquark states with the quantum number $J^{PC} = 2^{++}$. We construct both the diquark–antidiquark and mesonic–mesonic currents and calculate both their diagonal and off-diagonal correlation functions. Based on the obtained results, we further construct three mixing currents that are nearly non-correlated. We use one mixing current to extract the mass of the lowest-lying state to be $2.03^{+0.16}_{-0.15}$ GeV, which can be used to explain $f_2(2010)$ as a fully strange tetraquark state of $J^{PC} = 2^{++}$. This state was observed by BESIII in the $\phi\phi$ channel, and we propose to confirm it in the $\eta^{(\prime)}\eta^{(\prime)}$ channel.

KEYWORDS

exotic hadron, tetraquark state, QCD sum rules, Fierz rearrangement, interpolating current

1 Introduction

Many exotic hadrons were observed in particle experiments during the past 20 years [1], some of which are good candidates for the fully strange tetraquark states [2–22]. Especially the BESIII collaboration performed a partial wave analysis of the $J/\psi \to \gamma\phi\phi$ decay in 2016 [23]. They observed three tensor resonances, namely, $f_2(2010)$, $f_2(2300)$, and $f_2(2340)$ in the $\phi\phi$ invariant mass spectrum, whose masses and widths were measured to be

$$f_2(2010):\ M \approx 2011\ \text{MeV},\quad \Gamma \approx 202\ \text{MeV}; \tag{1}$$

$$f_2(2300):\ M \approx 2297\ \text{MeV},\quad \Gamma \approx 149\ \text{MeV}; \tag{2}$$

$$f_2(2340):\ M \approx 2339\ \text{MeV},\quad \Gamma \approx 319\ \text{MeV}. \tag{3}$$

These three resonances contain many strangeness components, so they are possible fully strange tetraquark states of $J^{PC} = 2^{++}$. With a large amount of the J/ψ sample, BESIII collaborations are still examining the physics happening in this energy region, and more rich-strangeness signals are expected in the coming future. Similar experiments can also be performed by Belle-II, COMPASS, GlueX, and PANDA, etc.

The fully strange tetraquark states are interesting from two aspects. Experimentally, their widths are possibly not very broad [possibly at the order of $\mathcal{O}(100\ \text{MeV})$], so they are capable of being observed. Theoretically, their internal structures are simpler than other tetraquark states due to the Pauli principle's restriction on identical strangeness quarks and antiquarks, which limits their potential number and makes them easier to be observed. In the past 15 years, we have applied the QCD sum rule method to study the fully strange tetraquark

states with quantum numbers $J^{PC} = 0^{-+}/1^{\pm\pm}/4^{+-}$ [24–32]. More theoretical studies can be found in [33–42].

In this paper, we shall study the fully strange tetraquark states with the quantum number $J^{PC} = 2^{++}$. We shall systematically construct both the diquark–antidiquark and mesonic–mesonic currents. We shall apply the method of QCD sum rules to study these currents as a whole, and extract the mass of the lowest-lying state to be $2.03^{+0.16}_{-0.15}$ GeV. Our results suggest that the $f_2(2010)$ can be explained as the fully strange tetraquark state of $J^{PC} = 2^{++}$, while it is not easy to interpret the $f_2(2300)$ and $f_2(2340)$ as such states.

This paper is organized as follows. In Section 2, we systematically construct the fully strange tetraquark states with the quantum number $J^{PC} = 2^{++}$. We use these currents to perform QCD sum rule analyses in Section 3, where we calculate both their diagonal and off-diagonal correlation functions. Based on the obtained results, we use the diquark–antidiquark currents to perform numerical analyses in Section 4, and we use their mixing currents to perform numerical analyses in Section 5. The obtained results are summarized and discussed in Section 6.

2 Interpolating currents

The fully strange tetraquark currents with quantum numbers $J^{PC} = 0^{-+}/1^{\pm\pm}/4^{+-}$ have been systematically constructed in [24–30, 43]. In this section, we follow the same approach to construct the fully strange tetraquark currents with the quantum number $J^{PC} = 2^{++}$. We observe three independent diquark–antidiquark currents.

$$\eta_1^{\mu\nu} = \mathcal{S}\left[s_a^T C\gamma^\mu s_b\ \bar{s}_a\gamma^\nu C\bar{s}_b^T\right], \tag{4}$$
$$\eta_2^{\mu\nu} = \mathcal{S}\left[s_a^T C\gamma^\mu\gamma_5 s_b\ \bar{s}_a\gamma^\nu\gamma_5 C\bar{s}_b^T\right], \tag{5}$$
$$\eta_3^{\mu\nu} = g_{\rho\sigma}\mathcal{S}\left[s_a^T C\sigma^{\mu\rho} s_b\ \bar{s}_a\sigma^{\nu\sigma} C\bar{s}_b^T\right], \tag{6}$$

where a and b are color indices, $C = i\gamma_2\gamma_0$ is the charge-conjugation operator, and the symbol $\mathcal{S}$ represents symmetrizing and subtracting trace terms in the set $\{\mu\nu\}$. Among these currents, $\eta_1^{\mu\nu}$ and $\eta_3^{\mu\nu}$ have the antisymmetric color structure $[ss]_{\bar{3}_C}[\bar{s}\bar{s}]_{3_C}$, and $\eta_2^{\mu\nu}$ has the symmetric color structure $[ss]_{6_C}[\bar{s}\bar{s}]_{\bar{6}_C}$, so the internal structure of $\eta_1^{\mu\nu}$ and $\eta_3^{\mu\nu}$ is more stable than that of $\eta_2^{\mu\nu}$. Moreover, the first current $\eta_1^{\mu\nu}$ only contains the S-wave diquark field $s_a^T C\gamma^\mu s_b$ and the S-wave antidiquark field $\bar{s}_a\gamma^\nu C\bar{s}_b^T$, so it has a more stable internal structure that may lead to a better sum rule result. In addition, the diquark field $s_a^T C\sigma^{\mu\nu} s_b$ of $J^P = 1^\pm$ contains both S- and P-wave components, so the third current $\eta_3^{\mu\nu}$ may also lead to a good sum rule result; the second current $\eta_2^{\mu\nu}$ contains the P-wave diquark field $s_a^T C\gamma^\mu\gamma_5 s_b$, so its predicted mass is probably larger. In the present study, we only consider tetraquark currents without derivatives, and more $J^{PC} = 2^{++}$ currents can be constructed when using derivatives. However, their internal structures are not so stable, and their predicted masses are probably also larger.

In addition to the aforementioned diquark–antidiquark currents, we find six mesonic–mesonic currents.

$$\xi_1^{\mu\nu} = \mathcal{S}\left[\bar{s}_a\gamma^\mu s_a\ \bar{s}_b\gamma^\nu s_b\right], \tag{7}$$
$$\xi_2^{\mu\nu} = \mathcal{S}\left[\bar{s}_a\gamma^\mu\gamma_5 s_a\ \bar{s}_b\gamma^\nu\gamma_5 s_b\right], \tag{8}$$
$$\xi_3^{\mu\nu} = g_{\rho\sigma}\mathcal{S}\left[\bar{s}_a\sigma^{\mu\rho} s_a\ \bar{s}_b\sigma^{\nu\sigma} s_b\right], \tag{9}$$
$$\xi_4^{\mu\nu} = \lambda_n^{ab}\lambda_n^{cd}\mathcal{S}\left[\bar{s}_a\gamma^\mu s_b\ \bar{s}_c\gamma^\nu s_d\right], \tag{10}$$
$$\xi_5^{\mu\nu} = \lambda_n^{ab}\lambda_n^{cd}\mathcal{S}\left[\bar{s}_a\gamma^\mu\gamma_5 s_b\ \bar{s}_c\gamma^\nu\gamma_5 s_d\right], \tag{11}$$
$$\xi_6^{\mu\nu} = \lambda_n^{ab}\lambda_n^{cd} g_{\rho\sigma}\mathcal{S}\left[\bar{s}_a\sigma^{\mu\rho} s_b\ \bar{s}_c\sigma^{\nu\sigma} s_d\right]. \tag{12}$$

We can verify the following relations through the Fierz rearrangement, so the number of independent mesonic–mesonic currents is also three.

$$\begin{pmatrix}\xi_4^{\mu\nu}\\ \xi_5^{\mu\nu}\\ \xi_6^{\mu\nu}\end{pmatrix} = \begin{pmatrix} -\frac{5}{3} & -1 & +1\\ -1 & -\frac{5}{3} & -1\\ +2 & -2 & -\frac{2}{3}\end{pmatrix}\begin{pmatrix}\xi_1^{\mu\nu}\\ \xi_2^{\mu\nu}\\ \xi_3^{\mu\nu}\end{pmatrix}. \tag{13}$$

Moreover, we can use the Fierz rearrangement to relate the diquark–antidiquark and mesonic–mesonic currents.

$$\begin{pmatrix}\eta_1^{\mu\nu}\\ \eta_2^{\mu\nu}\\ \eta_3^{\mu\nu}\end{pmatrix} = \begin{pmatrix} -\frac{1}{2} & +\frac{1}{2} & +\frac{1}{2}\\ +\frac{1}{2} & -\frac{1}{2} & +\frac{1}{2}\\ +1 & +1 & 0\end{pmatrix}\begin{pmatrix}\xi_1^{\mu\nu}\\ \xi_2^{\mu\nu}\\ \xi_3^{\mu\nu}\end{pmatrix}. \tag{14}$$

Therefore, the diquark–antidiquark and mesonic–mesonic constructions are equivalent to each other, when the local currents are investigated. We shall use this Fierz identity to study the decay behaviors at the end of this paper.

3 QCD sum rule analysis

The QCD sum rule method is a powerful and successful non-perturbative method [44, 45]. In this section, we apply it to study the currents $\eta_{1,2,3}^{\mu\nu}$ and calculate their two-point correlation functions

$$\begin{aligned}\Pi_{ij}^{\mu\nu,\mu'\nu'}(q^2) &\equiv i\int d^4x e^{iqx}\langle 0|\mathbf{T}\left[\eta_i^{\mu\nu}(x)\eta_j^{\mu'\nu',\dagger}(0)\right]|0\rangle\\ &= \Pi_{ij}(q^2)\times\mathcal{S}'\left[\tilde{g}^{\mu\mu'}\tilde{g}^{\nu\nu'}\right],\end{aligned} \tag{15}$$

at both the hadron and quark–gluon levels. Here, $\tilde{g}^{\mu\nu} = g^{\mu\nu} - q^\mu q^\nu/q^2$, and the symbol $\mathcal{S}'$ denotes symmetrizing and subtracting trace terms in the two sets $\{\mu\nu\}$ and $\{\mu'\nu'\}$, respectively.

At the hadron level, we generally assume that the currents $\eta_i^{\mu\nu}$ $(i = 1\cdots3)$ couple to the states X_n $(n = 1\cdots N)$ through

$$\langle 0|\eta_i^{\mu\nu}|X_n\rangle = f_{in}\epsilon^{\mu\nu}, \tag{16}$$

where f_{in} is the decay constant and $\epsilon^{\mu\nu}$ is the symmetric and traceless polarization tensor. Then, we use the dispersion relation to express $\Pi_{ij}(q^2)$ as

$$\Pi_{ij}(q^2) = \int_{s_<}^{\infty}\frac{\rho_{ij}^{\rm phen}(s)}{s - q^2 - i\varepsilon}ds, \tag{17}$$

where $s_< = 16m_s^2$ is the physical threshold and $\rho_{ij}^{\rm phen}(s)$ is the phenomenological spectral density. We parameterize it for the states X_n and a continuum contribution as

$$\begin{aligned}&\rho_{ij}^{\rm phen}(s)\times\mathcal{S}'\left[\tilde{g}^{\mu\mu'}\tilde{g}^{\nu\nu'}\right]\\ &= \sum_n\delta(s - M_n^2)\langle 0|\eta_i^{\mu\nu}|X_n\rangle\langle X_n|\eta_j^{\mu'\nu',\dagger}|0\rangle + \cdots\\ &= \sum_n f_{in}f_{jn}\delta(s - M_n^2)\times\mathcal{S}'\left[\tilde{g}^{\mu\mu'}\tilde{g}^{\nu\nu'}\right] + \cdots,\end{aligned} \tag{18}$$

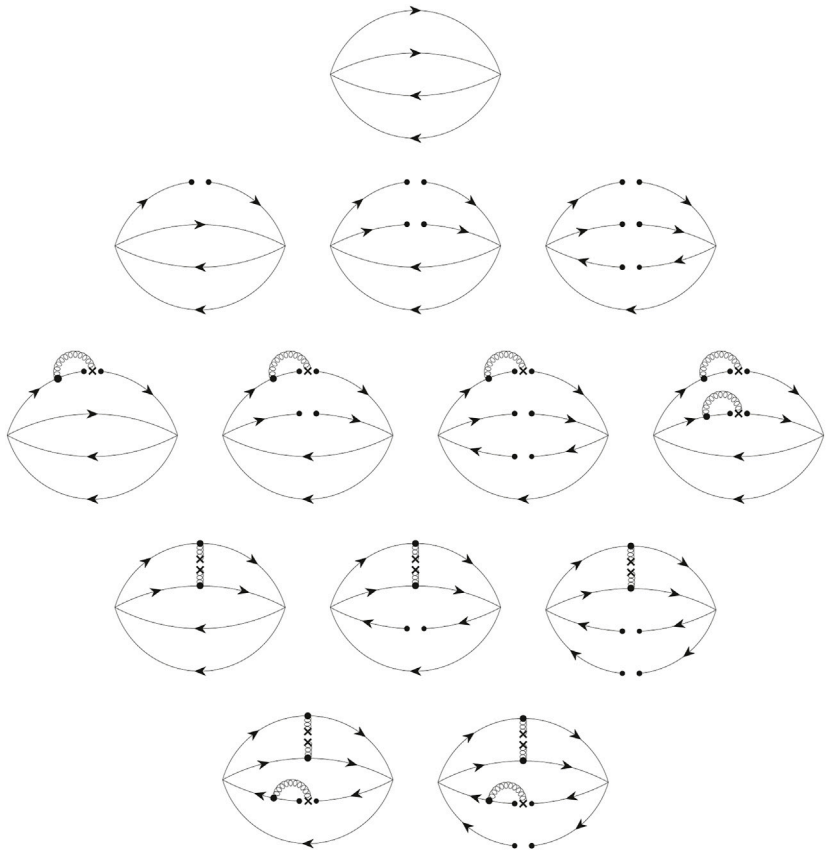

FIGURE 1
Feynman diagrams for the fully strange tetraquark currents of $J^{PC}=2^{++}$.

where M_n is the mass of X_n and $\cdots$ is contributed by the continuum. It should be noted that the widths of X_n are not taken into account in the present study, and the two-meson thresholds are also not taken into account, such as the $\phi\phi$ threshold. The Fierz rearrangement given in Eq. 13 indicates that the tetraquark currents $\eta^{\mu\nu}_{1,2,3}$ can easily couple to two mesons, which causes some difficulties in extracting the correct information about the resonance when the two-meson thresholds contribute significantly. The authors of [46] suggest that the four-quark diagrams with no singularity at $s=(\sum_{i=1}^{4}m_i)^2$ (m_i is the quark mass) are relevant to two free mesons but not relevant to the four-quark state. However, the validity of this criterion is still not clear.

At the quark–gluon level, we apply the method of the operator product expansion (OPE) to calculate Eq. 15 and extract the OPE spectral density $\rho_{ij}(s)\equiv\rho_{ij}^{\mathrm{OPE}}(s)$. In this study, we take into account the Feynman diagrams shown in Figure 1 and perform the calculations up to the twelfth dimension, where we consider the perturbative term, the strange quark mass m_s, the quark condensate $\langle\bar{s}s\rangle$, the double-gluon condensate $\langle g_s^2GG\rangle$, the quark–gluon mixed condensate $\langle g_s\bar{s}\sigma Gs\rangle$, and their combinations. We do not consider some other condensates, such as $\langle g_s\bar{s}D_\mu G^{\mu\nu}\gamma_\nu s\rangle$ and the diagrams with *up*/*down* quark loops, since their calculations are difficult. The vacuum saturation is assumed for higher-dimensional operators, *i.e.*, $\langle\bar{s}s\bar{s}s\rangle\approx\langle\bar{s}s\rangle^2$ and $\langle\bar{s}sg_s\bar{s}\sigma Gs\rangle\approx\langle\bar{s}s\rangle\langle g_s\bar{s}\sigma Gs\rangle$. We calculate all the diagrams proportional to $g_s^{N=0}$ and $g_s^{N=1}$, where we find the $D=6$ term $\langle\bar{s}s\rangle^2$ and the $D=8$ term $\langle\bar{s}s\rangle\langle g_s\bar{s}\sigma Gs\rangle$ to be important. We partly calculate the diagrams proportional to $g_s^{N\geq2}$, and we find their contributions to be small.

Finally, we perform the Borel transformation at both the hadron and quark–gluon levels. After approximating the continuum using $\rho_{ij}(s)$ above the threshold value s_0, we arrive at the sum rule equation

$$\begin{aligned}\Pi_{ij}(s_0,M_B^2)&=\sum_n f_{in}f_{jn}e^{-M_n^2/M_B^2}\\&=\int_{s_<}^{s_0}e^{-s/M_B^2}\rho_{ij}(s)ds.\end{aligned}\tag{19}$$

The explicit sum rule equations extracted from the currents $\eta^{\mu\nu}_{1,2,3}$ are as follows:

$$\begin{aligned}\Pi_{11}=&\int_{16m_s^2}^{s_0}e^{-s/M_B^2}ds\times\left[\frac{s^4}{86016\pi^6}-\frac{m_s^2s^3}{2880\pi^6}+\left(-\frac{11\langle g_s^2GG\rangle}{122880\pi^6}-\frac{3m_s\langle\bar{s}s\rangle}{320\pi^4}\right)s^2\right.\\&+\left(\frac{5\langle g_s^2GG\rangle m_s^2}{9216\pi^6}-\frac{7m_s\langle g_s\bar{s}\sigma Gs\rangle}{288\pi^4}+\frac{\langle\bar{s}s\rangle^2}{18\pi^2}\right)s\\&\left.+\frac{11\langle g_s^2GG\rangle m_s\langle\bar{s}s\rangle}{6912\pi^4}+\frac{5m_s^2\langle\bar{s}s\rangle^2}{24\pi^2}+\frac{7\langle\bar{s}s\rangle\langle g_s\bar{s}\sigma Gs\rangle}{144\pi^2}\right]\\&+\left(-\frac{\langle g_s^2GG\rangle\langle\bar{s}s\rangle^2}{432\pi^2}-\frac{4m_s\langle\bar{s}s\rangle^3}{9}+\frac{\langle g_s^2GG\rangle m_s\langle g_s\bar{s}\sigma Gs\rangle}{1152\pi^4}+\frac{m_s^2\langle\bar{s}s\rangle\langle g_s\bar{s}\sigma Gs\rangle}{4\pi^2}\right)\\&+\frac{1}{M_B^2}\left(\frac{5\langle g_s^2GG\rangle m_s^2\langle\bar{s}s\rangle^2}{3456\pi^2}+\frac{5m_s^2\langle g_s\bar{s}\sigma Gs\rangle^2}{288\pi^2}+\frac{5m_s\langle\bar{s}s\rangle^2\langle g_s\bar{s}\sigma Gs\rangle}{54}\right),\end{aligned}\tag{20}$$

$$\Pi_{22} = \int_{16m_s^2}^{s_0} e^{-s/M_B^2} ds \times \left[\frac{s^4}{43008\pi^6} - \frac{m_s^2 s^3}{360\pi^6} + \left(-\frac{19\langle g_s^2 GG\rangle}{122880\pi^6} + \frac{7m_s\langle \bar{s}s\rangle}{160\pi^4} \right) s^2 \right.$$
$$+ \left(-\frac{\langle \bar{s}s\rangle^2}{9\pi^2} + \frac{17m_s\langle g_s\bar{s}\sigma Gs\rangle}{288\pi^4} + \frac{11\langle g_s^2 GG\rangle m_s^2}{9216\pi^6} \right) s$$
$$\left. - \frac{17\langle \bar{s}s\rangle\langle g_s\bar{s}\sigma Gs\rangle}{144\pi^2} + \frac{7\langle g_s^2 GG\rangle m_s\langle \bar{s}s\rangle}{6912\pi^4} + \frac{7m_s^2\langle \bar{s}s\rangle^2}{4\pi^2} \right]$$
$$+ \left(\frac{m_s^2\langle \bar{s}s\rangle\langle g_s\bar{s}\sigma Gs\rangle^2}{2\pi^2} - \frac{\langle g_s^2 GG\rangle\langle \bar{s}s\rangle^2}{432\pi^2} \right.$$
$$\left. + \frac{\langle g_s^2 GG\rangle m_s\langle g_s\bar{s}\sigma Gs\rangle}{1152\pi^4} - \frac{8m_s\langle \bar{s}s\rangle^3}{9} \right)$$
$$+ \frac{1}{M_B^2} \left(\frac{7\langle g_s^2 GG\rangle m_s^2\langle \bar{s}s\rangle^2}{3456\pi^2} + \frac{65m_s\langle \bar{s}s\rangle^2\langle g_s\bar{s}\sigma Gs\rangle}{54} - \frac{13m_s^2\langle g_s\bar{s}\sigma Gs\rangle^2}{72\pi^2} \right), \tag{21}$$

$$\Pi_{33} = \int_{16m_s^2}^{s_0} e^{-s/M_B^2} ds \times \left[\frac{s^4}{43008\pi^6} - \frac{m_s^2 s^3}{576\pi^6} + \left(\frac{m_s\langle \bar{s}s\rangle}{80\pi^4} - \frac{\langle g_s^2 GG\rangle}{6144\pi^6} \right) s^2 + \frac{m_s^2\langle g_s^2 GG\rangle}{576\pi^6} s \right.$$
$$\left. + \frac{13m_s^2\langle \bar{s}s\rangle^2}{12\pi^2} - \frac{\langle g_s^2 GG\rangle m_s\langle \bar{s}s\rangle}{576\pi^4} \right] + \left(\frac{m_s^2\langle \bar{s}s\rangle\langle g_s\bar{s}\sigma Gs\rangle^2}{2\pi^2} - \frac{8m_s\langle \bar{s}s\rangle^3}{9} \right)$$
$$+ \frac{1}{M_B^2} \left(\frac{\langle g_s^2 GG\rangle m_s^2\langle \bar{s}s\rangle^2}{432\pi^2} + \frac{2m_s\langle \bar{s}s\rangle^2\langle g_s\bar{s}\sigma Gs\rangle}{3} - \frac{m_s^2\langle g_s\bar{s}\sigma Gs\rangle^2}{16\pi^2} \right), \tag{22}$$

$$\Pi_{12} = \int_{16m_s^2}^{s_0} e^{-s/M_B^2} ds \times \left[\frac{\langle g_s^2 GG\rangle}{40960\pi^6} s^2 - \frac{m_s^2\langle g_s^2 GG\rangle}{3072\pi^6} s + \frac{\langle g_s^2 GG\rangle m_s\langle \bar{s}s\rangle}{2304\pi^4} \right]$$
$$+ \frac{1}{M_B^2} \left(-\frac{\langle g_s^2 GG\rangle m_s^2\langle \bar{s}s\rangle^2}{1152\pi^2} \right), \tag{23}$$

$$\Pi_{13} = \int_{16m_s^2}^{s_0} e^{-s/M_B^2} ds \times \left[-\frac{m_s^2}{960\pi^6} s^3 + \frac{m_s\langle \bar{s}s\rangle}{32\pi^4} s^2 \right.$$
$$+ \left(\frac{5m_s\langle g_s\bar{s}\sigma Gs\rangle}{96\pi^4} + \frac{\langle g_s^2 GG\rangle m_s^2}{2304\pi^6} - \frac{\langle \bar{s}s\rangle^2}{9\pi^2} \right) s$$
$$\left. - \frac{\langle g_s^2 GG\rangle m_s\langle \bar{s}s\rangle}{384\pi^4} + \frac{2m_s^2\langle \bar{s}s\rangle^2}{3\pi^2} - \frac{5\langle \bar{s}s\rangle\langle g_s\bar{s}\sigma Gs\rangle}{48\pi^2} \right],$$
$$+ \left(\frac{\langle g_s^2 GG\rangle\langle \bar{s}s\rangle^2}{432\pi^2} - \frac{\langle g_s^2 GG\rangle m_s\langle g_s\bar{s}\sigma Gs\rangle}{1152\pi^4} \right)$$
$$+ \frac{1}{M_B^2} \left(\frac{\langle \bar{s}s\rangle^2 m_s\langle g_s\bar{s}\sigma Gs\rangle}{2} - \frac{5m_s^2\langle g_s\bar{s}\sigma Gs\rangle^2}{48\pi^2} \right), \tag{24}$$

$$\Pi_{23} = \int_{16m_s^2}^{s_0} e^{-s/M_B^2} ds \times \left[\left(\frac{m_s\langle g_s\bar{s}\sigma Gs\rangle}{96\pi^4} - \frac{\langle g_s^2 GG\rangle m_s^2}{768\pi^6} \right) s \right.$$
$$\left. + \frac{\langle g_s^2 GG\rangle m_s\langle \bar{s}s\rangle}{128\pi^4} - \frac{\langle \bar{s}s\rangle\langle g_s\bar{s}\sigma Gs\rangle}{48\pi^2} \right]$$
$$+ \left(\frac{\langle g_s^2 GG\rangle m_s\langle g_s\bar{s}\sigma Gs\rangle}{384\pi^4} - \frac{\langle g_s^2 GG\rangle\langle \bar{s}s\rangle^2}{144\pi^2} \right)$$
$$+ \frac{1}{M_B^2} \left(\frac{\langle \bar{s}s\rangle^2 m_s\langle g_s\bar{s}\sigma Gs\rangle}{18} - \frac{m_s^2\langle g_s\bar{s}\sigma Gs\rangle^2}{48\pi^2} \right). \tag{25}$$

For completeness, we have calculated both the diagonal and off-diagonal correlation functions. We shall investigate them using two steps, the single-channel analysis and the multi-channel analysis, in the following sections.

4 Single-channel analysis

In this section, we perform the single-channel analysis. To perform this, we simply neglect the off-diagonal correlation functions; *i.e.*, we assume $\rho_{ij}(s)|_{i\neq j} = 0$ so that only $\rho_{ii}(s) \neq 0$. Under this assumption, any two of the three currents $\eta^{\mu\nu}_{1,2,3}$ cannot mainly couple to the same state X; otherwise,

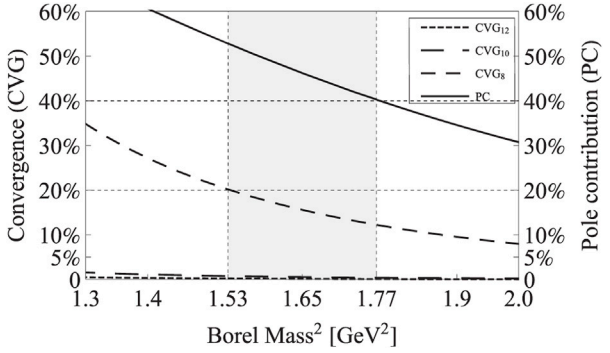

FIGURE 2
$CVG_{12/10/8}$ and PC with respect to the Borel mass M_B. These curves are obtained using the spectral density $\rho_{11}(s)$ given in Eq. 20, when setting s_0=6.5 GeV^2.

$$\rho_{ij}(s) \times \mathcal{S}' \left[\tilde{g}^{\mu\mu'} \tilde{g}^{\nu\nu'} \right]$$
$$= \sum_n \delta(s - M_n^2) \langle 0|\eta_i^{\mu\nu}|X_n\rangle\langle X_n|\eta_j^{\mu'\nu',\dagger}|0\rangle + \cdots$$
$$\approx \delta(s - M_X^2) \langle 0|\eta_i^{\mu\nu}|X\rangle\langle X|\eta_j^{\mu'\nu',\dagger}|0\rangle + \cdots$$
$$\neq 0. \tag{26}$$

This allows us to further assume that the three currents $\eta^{\mu\nu}_{1,2,3}$ couple separately to the three states $X_{1,2,3}$ through

$$\langle 0|\eta_i^{\mu\nu}|X_j\rangle = f_{ij}\epsilon^{\mu\nu}, \tag{27}$$

with $f_{ii} \neq 0$ and $f_{ij} = 0$ for $i, j = 1\cdots3$ and $i \neq j$.

Now, we can parameterize the diagonal spectral density $\rho_{ii}(s)$ as one-pole dominance for the state X_i and a continuum contribution. This simplifies Eq. 19 to be

$$\Pi_{ii}(s_0, M_B^2) = f_{ii}^2 e^{-M_i^2/M_B^2} = \int_{s_<}^{s_0} e^{-s/M_B^2} \rho_{ii}(s) ds. \tag{28}$$

It can be used to calculate M_i through

$$M_i^2(s_0, M_B) = \frac{\int_{s_<}^{s_0} e^{-s/M_B^2} s\rho_{ii}(s) ds}{\int_{s_<}^{s_0} e^{-s/M_B^2} \rho_{ii}(s) ds}. \tag{29}$$

We use the spectral density $\rho_{11}(s)$ given in Eq. 20 as an example to perform the single-channel numerical analysis. We take the following values for various sum rule parameters [1, 47–53]:

$$\begin{aligned} m_s(2\text{ GeV}) &= 93^{+11}_{-5}\text{ MeV}, \\ \langle g_s^2 GG\rangle &= (0.48 \pm 0.14)\text{ GeV}^4, \\ \langle \bar{s}s\rangle &= -(0.8 \pm 0.1) \times (0.240\text{ GeV})^3, \\ \langle g_s\bar{s}\sigma Gs\rangle &= -M_0^2 \times \langle \bar{s}s\rangle, \\ M_0^2 &= (0.8 \pm 0.2)\text{ GeV}^2. \end{aligned} \tag{30}$$

Equation 29 states that mass M_1 depends on two free parameters, the threshold value s_0, and the Borel mass M_B. We consider three aspects to determine their working regions: a) the convergence of OPE, b) the sufficient amount of pole contribution, and c) the stability of the mass dependence on these two parameters.

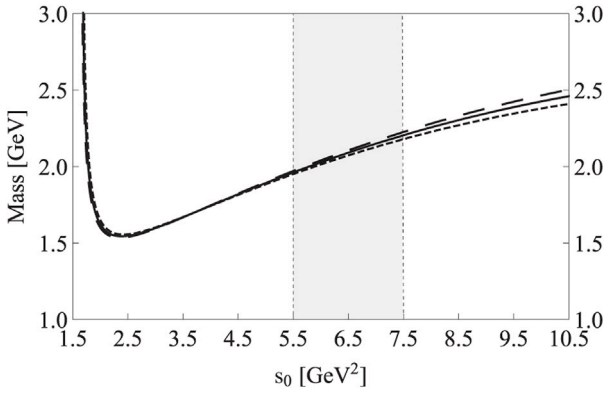

FIGURE 3
Mass M_1 of the state X_1 with respect to the threshold value s_0. Short-dashed/solid/long-dashed curves are obtained by setting M_B^2 = 1.53/1.65/1.77 GeV^2, respectively. These curves are obtained using the spectral density $\rho_{11}(s)$ given in Eq. 20.

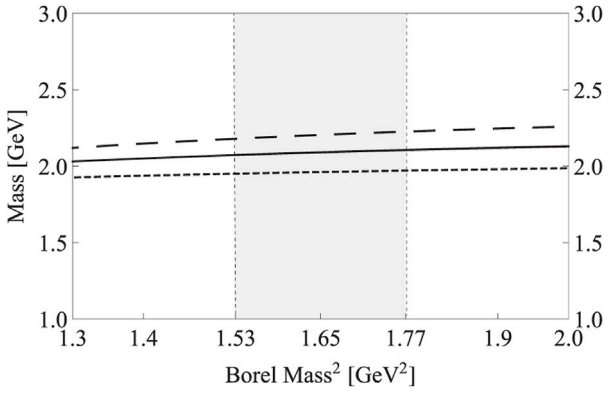

FIGURE 4
Mass M_1 of the state X_1 with respect to the Borel mass M_B. Short-dashed/solid/long-dashed curves are obtained by setting s_0=5.5/6.5/7.5 GeV^2, respectively. These curves are obtained using the spectral density $\rho_{11}(s)$ given in Eq. 20.

First, we investigate the convergence of OPE, which is the cornerstone of a reliable QCD sum rule analysis. We require the D = 12/10/8 terms to be less than 5%/10%/20%, respectively.

$$\mathrm{CVG}_{12} = \left|\frac{\Pi_{11}^{D=12}(\infty, M_B^2)}{\Pi_{11}(\infty, M_B^2)}\right| \leq 5\%, \tag{31}$$

$$\mathrm{CVG}_{10} = \left|\frac{\Pi_{11}^{D=10}(\infty, M_B^2)}{\Pi_{11}(\infty, M_B^2)}\right| \leq 10\%, \tag{32}$$

$$\mathrm{CVG}_{8} = \left|\frac{\Pi_{11}^{D=8}(\infty, M_B^2)}{\Pi_{11}(\infty, M_B^2)}\right| \leq 20\%. \tag{33}$$

Figure 2 shows that through the dashed curves, the lower bound of the Borel mass is determined to be $M_B^2 \geq 1.53$ GeV^2.

Second, we investigate the one-pole-dominance assumption by requiring the pole contribution to be larger than 40%:

TABLE 1 QCD sum rule results for the fully strange tetraquark states with the quantum number J^{PC} =2^{++}, extracted from the diquark–antidiquark currents $\eta_{1,2,3}^{\mu\nu}$ and their mixing currents $J_{1,2,3}^{\mu\nu}$.

Current	$s_0^{\min}$ [GeV^2]	Working regions		Pole [%]	Mass [GeV]
		M_B^2 [GeV^2]	s_0 [GeV^2]		
$\eta_1^{\mu\nu}$	5.4	1.53–1.77	6.5 ± 1.0	40–53	$2.09^{+0.19}_{-0.22}$
$\eta_2^{\mu\nu}$	12.4	2.19–2.65	13.5 ± 3.0	40–52	$3.49^{+0.36}_{-0.22}$
$\eta_3^{\mu\nu}$	6.2	1.24–1.43	7.0 ± 1.0	40–53	$2.19^{+0.20}_{-0.28}$
$J_1^{\mu\nu}$	5.6	1.71–1.81	6.0 ± 1.0	40–45	$2.03^{+0.16}_{-0.15}$
$J_2^{\mu\nu}$	12.7	2.16–2.78	14.0 ± 3.0	40–55	$3.58^{+0.39}_{-0.23}$
$J_3^{\mu\nu}$	12.2	2.19–2.69	13.5 ± 3.0	40–53	$3.44^{+0.32}_{-0.24}$

$$\text{Pole Contribution (PC)} = \left|\frac{\Pi_{11}(s_0, M_B^2)}{\Pi_{11}(\infty, M_B^2)}\right| \geq 40\%. \tag{34}$$

Figure 2 shows that through the solid curve, the upper bound of the Borel mass is determined to be $M_B^2 \leq 1.77$ GeV^2 when setting s_0 = 6.5 GeV^2. Altogether, we determine the Borel window to be 1.53 GeV$^2 \leq M_B^2 \leq 1.77$ GeV^2 for s_0 = 6.5 GeV^2. We redo the same procedures and find that there are non-vanishing Borel windows when $s_0 \geq s_0^{\min}$ = 5.4 GeV^2.

Third, we investigate the stability of the mass dependence on s_0 and M_B. As shown in Figure 3, we find a mass minimum around $s_0 \approx$ 3 GeV^2, and the mass dependence on s_0 is moderate inside the region 5.5 GeV$^2 \leq s_0 \leq$ 7.5 GeV^2. As shown in Figure 4, the mass dependence on M_B is rather weak inside the Borel window 1.53 GeV$^2 \leq M_B^2 \leq$ 1.77 GeV^2.

Altogether, we determine our working regions to be 5.5 GeV$^2 \leq s_0 \leq$ 7.5 GeV^2 and 1.53 GeV$^2 \leq M_B^2 \leq$ 1.77 GeV^2, where the mass of X_1 is calculated to be

$$M_1 = 2.09^{+0.19}_{-0.22}\ \text{GeV}. \tag{35}$$

Its central value is obtained by setting s_0 = 6.5 GeV^2 and M_B^2 = 1.65 GeV^2, and its uncertainty is due to the Borel mass M_B, the threshold value s_0, and various sum rule parameters listed in Eq. 30.

We follow the same procedures to study the other two currents, $\eta_2^{\mu\nu}$ and $\eta_3^{\mu\nu}$, separately. The obtained results are shown in Table 1. We shall further study the three currents $\eta_{1,2,3}^{\mu\nu}$ as a whole and perform the multi-channel analysis in the next section.

5 Multi-channel analyses

In this section, we perform the multi-channel analyses. To perform this, we do not neglect the off-diagonal correlation functions any more, *i.e.*, $\rho_{ij}(s)|_{i\neq j} \neq 0$. When setting s_0 = 6.0 GeV^2 and M_B^2 = 1.76 GeV^2, the 3 × 3 matrix $\Pi_{ij}(s_0, M_B^2)$ becomes

$$\Pi_{ij}(s_0, M_B^2) = \begin{pmatrix} 2.16 & 0.08 & -3.20 \\ 0.08 & -1.85 & 0.45 \\ -3.20 & 0.45 & 1.02 \end{pmatrix} \times 10^{-6}\ \text{GeV}^{14}. \tag{36}$$

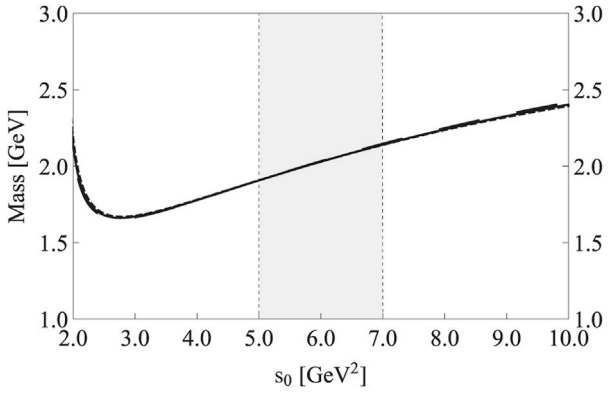

FIGURE 5
Mass M_1' of the state X_1' with respect to the threshold value s_0. Short-dashed/solid/long-dashed curves are obtained by setting M_B^2 = 1.71/1.76/1.81 GeV^2, respectively. These curves are obtained using the spectral density $\rho_{11}'(s)$ extracted from the mixing current $J_1^{\mu\nu}$.

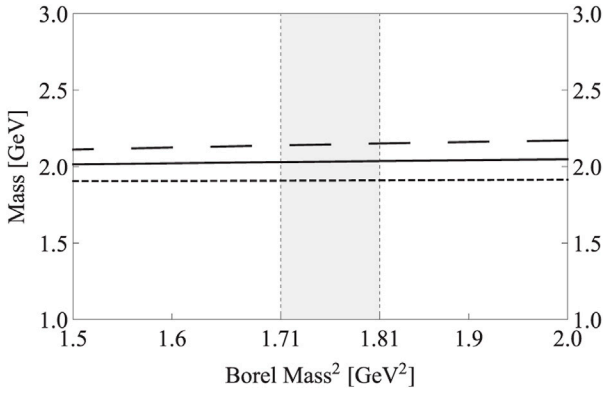

FIGURE 6
Mass M_1' of the state X_1' with respect to the Borel mass M_B. Short-dashed/solid/long-dashed curves are obtained by setting s_0=5.0/6.0/7.0 GeV^2, respectively. These curves are obtained using the spectral density $\rho_{11}'(s)$ extracted from the mixing current $J_1^{\mu\nu}$.

Therefore, $\eta_1^{\mu\nu}$ and $\eta_3^{\mu\nu}$ are strongly correlated with each other, and the off-diagonal terms are indeed non-negligible.

In order to diagonalize the 3 × 3 matrix $\Pi_{ij}(s_0, M_B^2)$, we construct three mixing currents $J_{1,2,3}^{\mu\nu}$

$$\begin{pmatrix} J_1^{\mu\nu} \\ J_2^{\mu\nu} \\ J_3^{\mu\nu} \end{pmatrix} = \mathbb{T}_{3\times3} \begin{pmatrix} \eta_1^{\mu\nu} \\ \eta_2^{\mu\nu} \\ \eta_3^{\mu\nu} \end{pmatrix}, \tag{37}$$

where $\mathbb{T}_{3\times3}$ is the transition matrix.

We use $\Pi_{ij}'(s_0, M_B^2)$ to denote the correlation functions extracted from the mixing currents $J_{1,2,3}^{\mu\nu}$. This 3 × 3 matrix becomes

$$\Pi_{ij}'(s_0, M_B^2) = \begin{pmatrix} 4.85 & 0 & 0 \\ 0 & -2.17 & 0 \\ 0 & 0 & -1.35 \end{pmatrix} \times 10^{-6}\ \text{GeV}^{14}, \tag{38}$$

when setting

$$\mathbb{T}_{3\times3} = \begin{pmatrix} 0.76 & -0.03 & -0.64 \\ -0.38 & 0.79 & -0.49 \\ 0.52 & 0.61 & 0.59 \end{pmatrix}, \tag{39}$$

as well as s_0 = 6.0 GeV^2 and M_B^2 = 1.76 GeV^2. Therefore, the off-diagonal terms of $\Pi_{ij}'(s_0, M_B^2)$ are negligible, and the three mixing currents $J_{1,2,3}^{\mu\nu}$ are nearly non-correlated around here. Moreover, the two correlation functions, $\Pi_{22}'(s_0, M_B^2)$ and $\Pi_{33}'(s_0, M_B^2)$, are both negative around $s \approx 6.0\,\text{GeV}^2$. This suggests that they are both non-physical around here, and the masses extracted from them should be significantly larger than $\sqrt{6.0}$ GeV ≈ 2.5 GeV.

Now, we can use the procedures applied in the previous section on the currents $\eta_{1,2,3}^{\mu\nu}$ to study their mixing currents $J_{1,2,3}^{\mu\nu}$. The obtained results are shown in Table 1. Particularly, the mass extracted from the current $J_1^{\mu\nu}$ is

$$M_1' = 2.03^{+0.16}_{-0.15}\ \text{GeV}, \tag{40}$$

as shown in Figures 5, 6 with respect to the threshold value s_0 and the Borel mass M_B.

6 Summary and discussions

In this paper, we use the QCD sum rule method to study the fully strange tetraquark states with the quantum number $J^{PC} = 2^{++}$. We systematically construct their interpolating currents and find three independent diquark–antidiquark currents, denoted as $\eta_{1,2,3}^{\mu\nu}$. We calculate both their diagonal and off-diagonal correlation functions. Based on the obtained results, we construct three mixing currents that are nearly non-correlated and denoted as $J_{1,2,3}^{\mu\nu}$. We use both the diquark–antidiquark currents $\eta_{1,2,3}^{\mu\nu}$ and the mixing currents $J_{1,2,3}^{\mu\nu}$ to perform QCD sum rule analyses. The obtained results are shown in Table 1.

Particularly, we use the mixing current $J_1^{\mu\nu}$ to evaluate the mass of the lowest-lying state to be $2.03^{+0.16}_{-0.15}$ GeV, while the masses extracted from the other two mixing currents, $J_2^{\mu\nu}$ and $J_3^{\mu\nu}$, are significantly larger than 3.0 GeV. The fully strange tetraquark states of $J^{PC} = 2^{++}$ naturally decay into the $\phi\phi$ channel, where the BESIII collaboration observed three tensor resonances, namely, $f_2(2010)$, $f_2(2300)$, and $f_2(2340)$ [23]. Accordingly, our results suggest that the $f_2(2010)$ can be explained as the fully strange tetraquark state of $J^{PC} = 2^{++}$, while it is not easy to interpret the $f_2(2300)$ and $f_2(2340)$ as such states.

In this paper, we also systematically construct the fully strange mesonic–mesonic currents of $J^{PC} = 2^{++}$, which can be related to the diquark–antidiquark currents through the Fierz rearrangement. In particular, we can apply Eqs. 37 and 39, and Eq. 14 to transform the mixing current $J_1^{\mu\nu}$ to be

$$J_1^{\mu\nu} = -1.04\ \xi_1^{\mu\nu} - 0.25\ \xi_2^{\mu\nu} + 0.37\ \xi_3^{\mu\nu}. \tag{41}$$

This Fierz identity suggests that the lowest-lying state dominantly decays into the S-wave $\phi(1020)\phi(1020)$ channel through the mesonic–mesonic current $\xi_1^{\mu\nu}$, while it can also decay into the D-wave $\eta^{(\prime)}\eta^{(\prime)}$ channel through $\xi_2^{\mu\nu}$. Accordingly, we propose to confirm the $f_2(2010)$ in the $\eta^{(\prime)}\eta^{(\prime)}$ channel in the future Belle-II, BESIII, COMPASS, GlueX, and PANDA experiments. In addition, more possible decay patterns can be obtained by annihilating an $s\bar{s}$ pair into a gluon, which then transits into the final states with a pair of strange mesons, such as $K\bar{K}$.

Data availability statement

The original contributions presented in the study are included in the article/Supplementary Material; further inquiries can be directed to the corresponding authors.

Author contributions

All authors listed have made a substantial, direct, and intellectual contribution to the work and approved it for publication.

Funding

This project was supported by the National Natural Science Foundation of China under grant no. 12075019, the Jiangsu Provincial Double-Innovation Program under grant no. JSSCRC2021488, and the Fundamental Research Funds for the Central Universities.

Conflict of interest

The authors declare that the research was conducted in the absence of any commercial or financial relationships that could be construed as a potential conflict of interest.

Publisher's note

All claims expressed in this article are solely those of the authors and do not necessarily represent those of their affiliated organizations, or those of the publisher, the editors, and the reviewers. Any product that may be evaluated in this article, or claim that may be made by its manufacturer, is not guaranteed or endorsed by the publisher.

References

1. Zyla PA, Barnett RM, Beringer J, Dahl O, Dwyer DA, Groom DE, et al. Review of particle physics. *PTEP* (2020) 2020(8):083C01. doi:10.1093/ptep/ptaa104

2. Chen H-X, Chen W, Liu X, Zhu S-L. The hidden-charm pentaquark and tetraquark states. *Phys Rept* (2016) 639:1–121. doi:10.1016/j.physrep.2016.05.004

3. Liu Y-R, Chen H-X, Chen W, Liu X, Zhu S-L. Pentaquark and tetraquark states. *Prog Part Nucl Phys* (2019) 107:237–320. doi:10.1016/j.ppnp.2019.04.003

4. Chen H-X, Chen W, Liu X, Liu Y-R, Zhu S-L. An updated review of the new hadron states. *Rept Prog Phys* (2023) 86(2):026201. doi:10.1088/1361-6633/aca3b6

5. Lebed RF, Mitchell RE, Swanson ES. Heavy-quark QCD exotica. *Prog Part Nucl Phys* (2017) 93:143–94. doi:10.1016/j.ppnp.2016.11.003

6. Esposito A, Pilloni A, Polosa AD. Multiquark resonances. *Phys Rept* (2017) 668:1–97. doi:10.1016/j.physrep.2016.11.002

7. Hosaka A, Iijima T, Miyabayashi K, Sakai Y, Yasui S. Exotic hadrons with heavy flavors: X, Y, Z, and related states. *PTEP* (2016) 2016(6):062C01. doi:10.1093/ptep/ptw045

8. Guo F-K, Hanhart C, Meißner U-G, Wang Q, Zhao Q, Zou B-S. Hadronic molecules. *Rev Mod Phys* (2018) 90(1):015004. doi:10.1103/RevModPhys.90.015004

9. Ali A, Lange JS, Stone S. Exotics: Heavy pentaquarks and tetraquarks. *Prog Part Nucl Phys* (2017) 97:123–98. doi:10.1016/j.ppnp.2017.08.003

10. Olsen SL, Skwarnicki T, Zieminska D. Nonstandard heavy mesons and baryons: Experimental evidence. *Rev Mod Phys* (2018) 90(1):015003. doi:10.1103/RevModPhys.90.015003

11. Karliner M, Rosner JL, Skwarnicki T. Multiquark states. *Ann Rev Nucl Part Sci* (2018) 68:17–44. doi:10.1146/annurev-nucl-101917-020902

12. Bass SD, Moskal P. η' and η mesons with connection to anomalous glue. *Rev Mod Phys* (2019) 91(1):015003. doi:10.1103/RevModPhys.91.015003

13. Brambilla N, Eidelman S, Hanhart C, Nefediev A, Shen C-P, Thomas CE, et al. The *XYZ* states: Experimental and theoretical status and perspectives. *Phys Rept* (2020) 873:1–154. doi:10.1016/j.physrep.2020.05.001

14. Guo F-K, Liu X-H, Sakai S. Threshold cusps and triangle singularities in hadronic reactions. *Prog Part Nucl Phys* (2020) 112:103757. doi:10.1016/j.ppnp.2020.103757

15. Ketzer B, Grube B, Ryabchikov D. Light-meson spectroscopy with COMPASS. *Prog Part Nucl Phys* (2020) 113:103755. doi:10.1016/j.ppnp.2020.103755

16. Yang G, Ping J, Segovia J. Tetra- and penta-quark structures in the constituent quark model. *Symmetry* (2020) 12(11):1869. doi:10.3390/sym12111869

17. Roberts CD, Richards DG, Horn T, Chang L. Insights into the emergence of mass from studies of pion and kaon structure. *Prog Part Nucl Phys* (2021) 120:103883. doi:10.1016/j.ppnp.2021.103883

18. Fang S-S, Kubis B, Kupść A. What can we learn about light-meson interactions at electron-positron colliders? *Prog Part Nucl Phys* (2021) 120:103884. doi:10.1016/j.ppnp.2021.103884

19. Jin S, Shen X. Highlights of light meson spectroscopy at the BESIII experiment. *Natl Sci Rev* (2021) 8(11):nwab198. doi:10.1093/nsr/nwab198

20. Albaladejo M, Bibrzycki L, Dawid SM, Fernandez-Ramirez C, Gonzalez-Solis S, Hiller Blin AN, et al. Novel approaches in hadron spectroscopy (2021). Available at: https://arxiv.org/abs/2112.13436 (Accessed December 26, 2021).

21. Meng L, Wang B, Wang G-J, Zhu S-L. Chiral perturbation theory for heavy hadrons and chiral effective field theory for heavy hadronic molecules. Available at: https://arxiv.org/abs/2204.08716 (Accessed April 19, 2022).

22. Brambilla N, Chen H-X, Esposito A, Ferretti J, Francis A, Guo F-K, et al. Substructure of multiquark hadrons (snowmass 2021 white paper). Available at: https://arxiv.org/abs/2203.16583 (Accessed March 30, 2022).

23. Ablikim M, Achasov M, Ai X, Albayrak O, Albrecht M, Ambrose D, et al. Observation of pseudoscalar and tensor resonances in $J/\psi \to \gamma\phi\phi$. *Phys Rev D* (2016) 93(11):112011. doi:10.1103/PhysRevD.93.112011

24. Chen H-X, Liu X, Hosaka A, Zhu S-L. Y(2175) state in the QCD sum rule. *Phys Rev D* (2008) 78:034012. doi:10.1103/PhysRevD.78.034012

25. Chen H-X, Hosaka A, Zhu S-L. $I^GJ^{PC} = 1^-1^{-+}$ tetraquark states. *Phys Rev D* (2008) 78:054017. doi:10.1103/PhysRevD.78.054017

26. Chen H-X, Hosaka A, Zhu S-L. $I^GJ^{PC} = 0^+1^{-+}$ tetraquark states. *Phys Rev D* (2008) 78:117502. doi:10.1103/PhysRevD.78.117502

27. Chen H-X, Shen C-P, Zhu S-L. Possible partner state of the *Y*(2175). *Phys Rev D* (2018) 98(1):014011. doi:10.1103/PhysRevD.98.014011

28. Cui E-L, Yang H-M, Chen H-X, Chen W, Shen C-P. QCD sum rule studies of $$s s {\bar{s}} {\bar{s}}$$ s s s s⁻s⁻tetraquark states with $$J{PC} = 1{+-}$$ J PC = 1 + -s s {\bar{s}} {\bar{s}} tetraquark states with $J^{PC} = 1^{+-}$. *Eur Phys J C* (2019) 79(3):232. doi:10.1140/epjc/s10052-019-6755-y

29. Dong R-R, Su N, Chen H-X, Cui E-L, Zhou Z-Y. QCD sum rule studies on the $$s s {\bar{s}} {\bar{s}}$$ tetraquark states of $$J{PC} = 0{-+}$$s s \bar{s} \bar{s} tetraquark states of $J^{PC} = 0^{-+}$. *Eur Phys J C* (2020) 80(8):749. doi:10.1140/epjc/s10052-020-8340-9

30. Dong R-R, Su N, Chen H-X. Highly excited and exotic fully-strange tetraquark states. *Eur Phys J C* (2022) 82(11):983. doi:10.1140/epjc/s10052-022-10955-0

31. Chen H-X, Chen W, Liu X, Liu X-H. Establishing the first hidden-charm pentaquark with strangeness. *Eur Phys J C* (2021) 81(5):409. doi:10.1140/epjc/s10052-021-09196-4

32. Chen H-X. Hadronic molecules in *B* decays. *Phys Rev D* (2022) 105(9):094003. doi:10.1103/PhysRevD.105.094003

33. Wang Z-G. Analysis of as a tetraquark state with QCD sum rules. *Nucl Phys A* (2007) 791:106–16. doi:10.1016/j.nuclphysa.2007.04.012

34. Wang Z-G. Light tetraquark state candidates. *Adv High Energ Phys.* (2020) 2020:1–7. doi:10.1155/2020/6438730

35. Agaev SS, Azizi K, Sundu H. Nature of the vector resonance *Y*(2175). *Phys Rev D* (2020) 101(7):074012. doi:10.1103/PhysRevD.101.074012

36. Azizi K, Agaev SS, Sundu H. Light axial-vector and vector resonances *X*(2100) and *X*(2239. *Nucl Phys B* (2019) 948:114789. doi:10.1016/j.nuclphysb.2019.114789

37. Pimikov AV. Nonlocal gluon condensates in QCD sum rules. *Phys Rev D* (2022) 106(5):056011. doi:10.1103/PhysRevD.106.056011

38. Liu F-X, Liu M-S, Zhong X-H, Zhao Q. Fully-strange tetraquark ss\bar{s}\bar{s} spectrum and possible experimental evidence. *Phys Rev D* (2021) 103(1):016016. doi:10.1103/PhysRevD.103.016016

39. Lü Q-F, Wang K-L, Dong Y-B. The tetraquark states and the structure of X(2239) observed by the BESIII collaboration *ss \bar{s} \bar{s} tetraquark states and the newly observed structure *X*(2239) by BESIII Collaboration. *Chin Phys C* (2020) 44(2):024101. doi:10.1088/1674-1137/44/2/024101

40. Deng C, Ping J, Wang F, Goldman T. Tetraquark state and multibody interaction. *Phys Rev D* (2010) 82:074001. doi:10.1103/PhysRevD.82.074001

41. Drenska NV, Faccini R, Polosa AD. Higher tetraquark particles. *Phys Lett B* (2008) 669:160–6. doi:10.1016/j.physletb.2008.09.038

42. Ebert D, Faustov RN, Galkin VO. Masses of light tetraquarks and scalar mesons in the relativistic quark model. *Eur Phys J C* (2009) 60:273–8. doi:10.1140/epjc/s10052-009-0925-2

43. Su N, Chen H-X. *S*- and *P*-wave fully strange tetraquark states from QCD sum rules. *Phys Rev D* (2022) 106(1):014023. doi:10.1103/PhysRevD.106.014023

44. Shifman MA, Vainshtein AI, Zakharov VI. QCD and resonance physics. theoretical foundations. *Nucl Phys B* (1979) 147:385–447. doi:10.1016/0550-3213(79)90022-1

45. Reinders LJ, Rubinstein H, Yazaki S. Hadron properties from QCD sum rules. *Phys Rept* (1985) 127:1–97. doi:10.1016/0370-1573(85)90065-1

46. Lucha W, Melikhov D, Sazdjian H. Tetraquark-adequate formulation of QCD sum rules. *Phys Rev D* (2019) 100(1):014010. doi:10.1103/PhysRevD.100.014010

47. Yang K-C, Hwang WYP, Henley EM, Kisslinger LS. QCD sum rules and neutron-proton mass difference. *Phys Rev D* (1993) 47:3001–12. doi:10.1103/PhysRevD.47.3001

48. Narison S. *QCD as a theory of hadrons: From partons to confinement*. Oxford, UK: Oxford University Press (2005).

49. Gimenez V, Lubicz V, Mescia F, Porretti V, Reyes J. Operator product expansion and quark condensate from lattice QCD in coordinate space. *Eur Phys J C* (2005) 41:535–44. doi:10.1140/epjc/s2005-02250-9

50. Jamin M. Flavour-symmetry breaking of the quark condensate and chiral corrections to the Gell-Mann–Oakes–Renner relation. *Phys Lett B* (2002) 538:71–6. doi:10.1016/S0370-2693(02)01951-2

51. Ioffe BL, Zyablyuk KN. Gluon condensate in charmonium sum rules with three-loop corrections. *Eur Phys J C* (2003) 27:229–41. doi:10.1140/epjc/s2002-01099-8

52. Ovchinnikov AA, Pivovarov AA. QCD sum rule calculation of the quark gluon condensate. *Sov J Nucl Phys* (1988) 48:721–3.

53. Ellis JR, Gardi E, Karliner M, Samuel MA. Renormalization-scheme dependence of Padé summation in QCD. *Phys Rev D* (1996) 54:6986–96. doi:10.1103/PhysRevD.54.6986